Fluxon-antifluxon state in stacked Josephson junctions

G. Carapella
Unità INFM and Dipartimento di Fisica, Università di Salerno, I-84081 Baronissi, Italy
(Received 17 July 1998)

The zero-field singularities that account for the oscillatory motion of bound fluxon-antifluxon pairs in stacks of two long Josephson junctions are investigated in detail. Experimental results concerning the *I-V* characteristics and the stability of the bound state are compared with existing theoretical models and with numerical results of a recent, more realistic, model. The microwave emission from the state is also described and discussed. [S0163-1829(99)13001-7]

I. INTRODUCTION

The physical system consisting of two stacked long Josephson junctions has been extensively investigated in recent years, both theoretically[1–10] and experimentally,[11–19] due to the variety of synchronization phenomena of the fluxon motion exhibited by the device, useful to the improvement of the existing fluxon oscillators, and due to the strong similarity with the basic structure of some superconducting materials (Bi-Sr-Ca-Cu-O family).

The coupled sine-Gordon equations that model the device predict the existence of two basic solitonic solutions describing a fluxon-antifluxon pair and a fluxon-fluxon pair, respectively. In the absence of magnetic field these solutions should be manifested in the *I-V* characteristic of the stack as current singularities with two different asymptotic voltages, the lower one corresponding to the antipolar state and the higher one to the homopolar state. Though predicted and theoretically investigated, the current singularities corresponding to the fluxon-antifluxon pairs were experimentally reported[15] only two years ago. For clarity, we remind the reader of some relevant experimental results[15–17] and we report further experimental investigation of the fluxon-antifluxon state; moreover, we try a systematic comparison with numerical and analytical results of the existing inductive model and with numerical results of a recently proposed[20] refinement of the model that accounts for the nonuniform current distribution in the electrodes of the real device. This refinement was proposed to account for some mutual interaction phenomena observed[20] when both junctions or only one junction in the stack was in the zero-voltage state in the absence of magnetic field. Due to the strict relation between the amplitude of current singularities and the Josephson critical current, the model is expected to describe quantitatively also the behavior of the fluxon-antifluxon state.

The paper is organized as follows. In Sec. II we provide the outline of the fabrication procedure of the samples, as it required some innovative techniques. In Sec. III the *I-V* experimental characteristic of the fluxon-antifluxon state is investigated and compared with the theory, while the stability of the state is covered in Sec. IV. Microwave radiation that we received from the state is finally discussed in Sec. V.

II. SAMPLES

The samples were fabricated using standard films deposition and photolithographic techniques, but the junction area was patterned using a novel procedure. An outline of the fabrication process that we will name ''overlap definition process (ODEP),'' is shown in Fig. 1. rf-sputtered Nb is patterned with the base electrode geometry (steps 1 and 2 in Fig. 1) by reactive ion etching (RIE) with a mixture of CF_4 (90%) and O_2 (10%). Then, for the sake of planarization, a self-aligned SiO_2 film with thickness comparable to the thickness of the base electrode is deposited by sputtering (steps 3 and 4 in Fig. 1). After a sputter cleaning of the base Nb, an Al layer ($\approx$5nm thick) is deposited on the whole substrate and oxidized thermally to form a $\approx$2-nm-thick Al_2O_3 oxide barrier, then another $\approx$2-nm-thick Al layer is sputtered. On the top of this we sputter a Nb film that is going to constitute finally the intermediate electrode of the device; therefore, its thickness was varied depending on the desired coupling. Note that the $Al/Al_2O_3/Al'/Nb$ structure (step 5 in Fig. 1) is fabricated without breaking the vacuum, to assure a good insulating barrier, and is deposited over a practically flat surface to prevent the eventual fracture of the intermediate electrode in the case of very thin Nb film.

The $Al/Al_2O_3/Al'/Nb$ structure is then patterned with the middle electrode geometry (steps 6 to 8 in Fig. 1) by using RIE to etch the Nb film (step 7) and a KOH solution to etch the $Al/Al_2O_3/Al'$ residual structure. At this point (step 8 in Fig. 1), we have the first junction of the stack, whose area is defined by the overlap of the bilayer and the base Nb film (this justifies the name ODEP for the process). Steps 1–8 could also be used to make single junctions. We investigated single junctions obtained with this process and we found that the insulating barrier had good quality and the dynamics (zero field steps) was systematically present in long junctions.

To make the second junction, first (step 9) we insulate the base Nb electrode with Nb_2O_5 obtained by wet anodization of the area unprotected by the photoresist of step 8 in Fig. 1. The old resist is removed with acetone and a new resist mask is defined with the geometry of the top electrode (step 10). The alignment of the photoresist edge with the base electrode edge in this step is only achieved within the resolution of the photolitographic process ($\approx 2\mu$m). The second junction is then obtained by deposition (step 11) of an $Al/Al_2O_3/Al'/Nb$

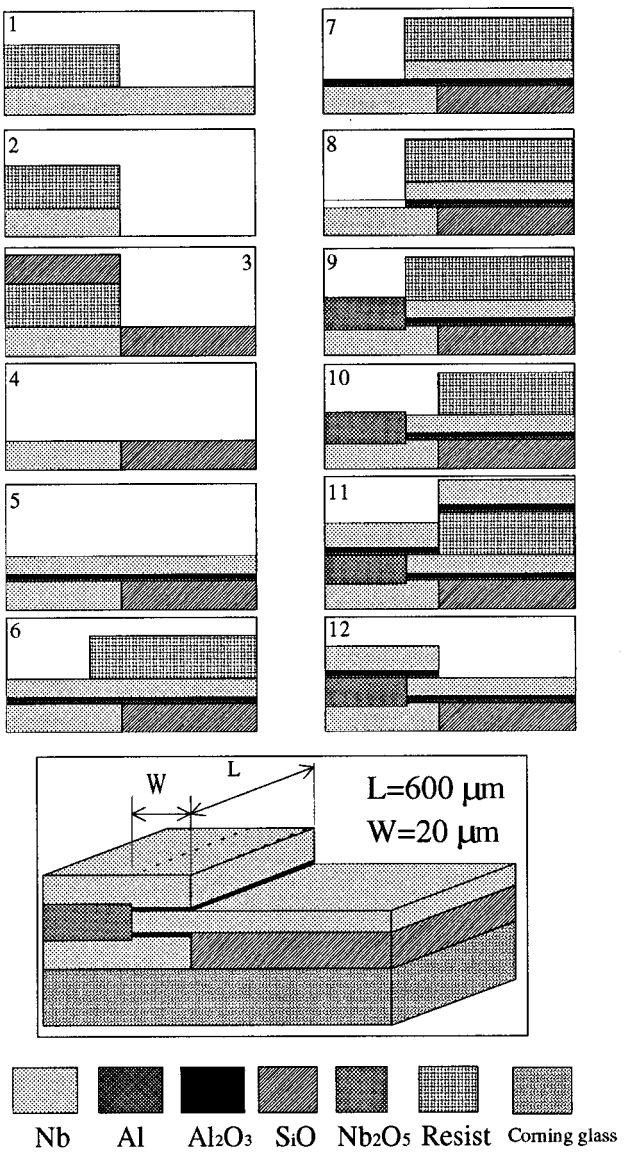

FIG. 1. Top: Outline of the ODEP process. Patterning of the base electrode (1, 2); self-aligned planarization process (3, 4); fabrication of barrier and intermediate electrode (5); patterning of the bottom junction (6, 7, 8); anodic oxidation of the base Nb film (9); fabrication of the top junction by liftoff technique (10, 11, 12). Bottom: Stack with ''double overlap'' geometry.

structure (as described above), which is patterned with the geometry of the top electrode using the lift-off (step 12) technique, and the stack is finally complete.

We fabricated stacks with $\approx$300-nm-thick outer electrodes and $\approx$60-nm or $\approx$30-nm-thick intermediate electrodes. Due to the backsputtering and the vacuum breaking present in the fabrication process, London penetration depth λ_L in our Nb was estimated (from measurement performed on single junctions) to be about 100nm, i.e., larger than the typical 80-nm value of rf-sputtered Nb films. Also the subgap current is quite large (the subgap resistance R_{sg} measured at 2mV was typically $\approx 0.5\Omega$), but this turns out to be a good feature, because the larger the damping, the smaller are the instability regions of the subgap quasiparticle curve (McCumber curve). The critical currents of the junctions (as estimated from the current rise to the gap sum voltage) was normally found to be the same within 10%, and of the order of 70A/cm^2. In all of the investigated stacks with the ''double overlap'' geometry shown in Fig. 1, the junctions have physical dimension $L \times W = (600 \times 20)\mu\text{m}^2$ and the typical Josephson penetration length λ_J is larger than 40μm, so that we have long and narrow junctions. In the three samples on which we report here, the magnetic coupling[8] ε and the normalized lengths of the junctions (see Sec. III for definitions) were $\varepsilon = -0.42$, $l_A \approx l_B = 15$, $\varepsilon = -0.56$, $l_A \approx l_B = 13$, $\varepsilon = -0.89$, $l_A \approx l_B = 10$, respectively. The samples were fabricated at the University of Salerno, Italy, and measured at the Technical University of Denmark, Denmark. The resolution of the voltage measurements was about 200nV and the resolution of current measurements was about 1μA.

III. *I-V* CHARACTERISTIC OF THE FLUXON-ANTIFLUXON STATE

In the absence of magnetic field, by sweeping the bias current of either of the two junctions in the lower region of the McCumber curve while the other junction is biased with constant current on the zero-voltage state or on the McCumber curve, it is possible to switch to a state where the junctions take the same voltage value. When the junctions are in this state, a variation of the bias current in one junction results in a variation of the common voltage value (voltage locking); this state exists for a finite range of the bias currents and common voltages (current steps). For the sake of clarity, the relevant experimental results[15–17] concerning this phenomenon, which we reported in Ref. 15, are summarized in Figs. 2 and Fig. 3.

At the top of Fig. 2 is shown the *I-V* characteristic of junction *B* while junction *A* is biased with a constant current. The magnification of the low-voltage region shows three steps that we named zero-field steps (ZFS's). On these steps, the voltage of the junction *A*, biased with constant current, follows exactly the voltage of junction *B*. This is better seen in the bottom of Fig. 2. Note that in the experiments the intermediate electrode was grounded (see inset at the top of Fig. 2) and we are referring voltage and bias polarities to this electrode. In Fig. 3 we report from Refs. 15–17 the *I-V* curves of ZFS1 seen in junction *B* using the current in junction *A* as a parameter: as the current in junction *A* is increased, the curves shift toward the bottom; an instability region appears in the lower branch of the step when the current in junction *A* is further increased; all the curves essentially fall on the top of each other if represented with a ''mean current'' axis defined by $I_s = (I_A + I_B)/2$.

Figures 2 and 3 refer to a stack with $\varepsilon = -0.56$ where the asymptotic voltage of ZFS1 is $V_{ZFS1} = 19.5\mu$V. In the same stack we can record up to six ZFS's and similar results are obtained reversing the role of the junctions. Moreover, the ZFS's exhibit similar features also in stacks with different values of the coupling constant ε, as is seen in Fig. 4 that refers to a stack with $\varepsilon = -0.42$ and to a stack with $\varepsilon = -0.89$. The asymptotic voltages are $V_{ZFS1} = 22.8\mu$V and $V_{ZFS1} = 10.8\mu$V, respectively. For the stack with $\varepsilon = -0.89$ we plotted also ZFS2 and replotted it using the mean current axis in the inset. The result suggests that also higher-order steps are driven by a force proportional to $I_s = (I_A + I_B)/2$.

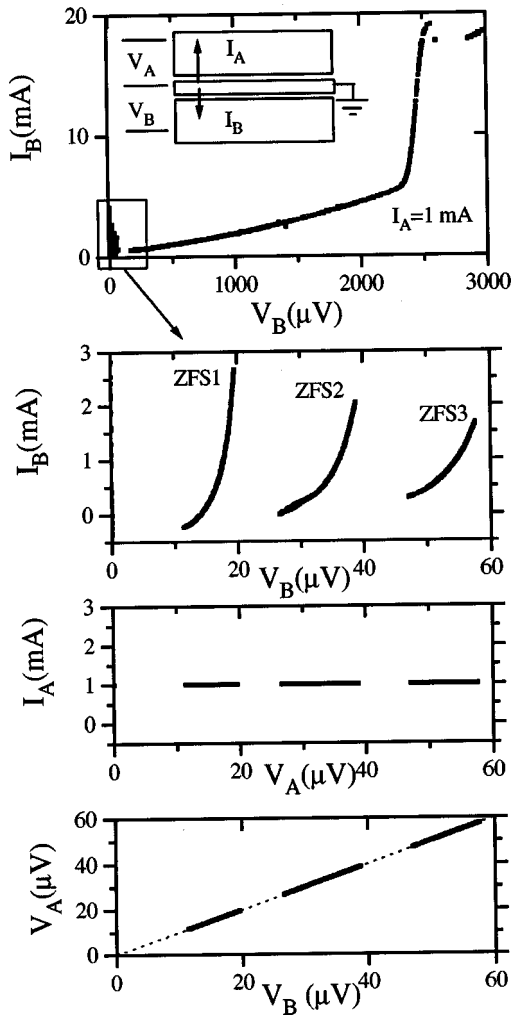

FIG. 2. From top to the bottom: I-V characteristic of the junction B for junction A at $I_A=1$mA; magnification of the low voltage region exhibiting three ZFS's; voltage of junction A while B is swept on these steps; voltage in junction A as a function of the voltage in junction B. The coupling constant of this stack is $\varepsilon=-0.56$.

All of the three voltage spacings of the ZFS's are found to be two times the voltage spacings of the Fiske steps of the c^- family,[14]

$$\Delta V^-_{ZFS}=2\times\Delta V^-_{FS}=2\times\frac{c^-}{2L}\Phi_0, \tag{1}$$

as we would expect for an oscillatory soliton motion with asymptotic velocity c^-.

The global picture, also taking into account the voltage polarities used, indicates that the oscillating solitons are fluxon-antifluxon pairs (a fluxon in a junction and an antifluxon in the other) in ZFS1, two pairs in ZFS2, and so on. In other words, we are concerned with the bunched fluxon-antifluxon state theoretically investigated extensively[3–7] and experimentally demonstrated in Ref. 15.

A. Comparison with the theory

The coupled sine-Gordon system equations describing the stack of two long Josephson junctions have been extensively

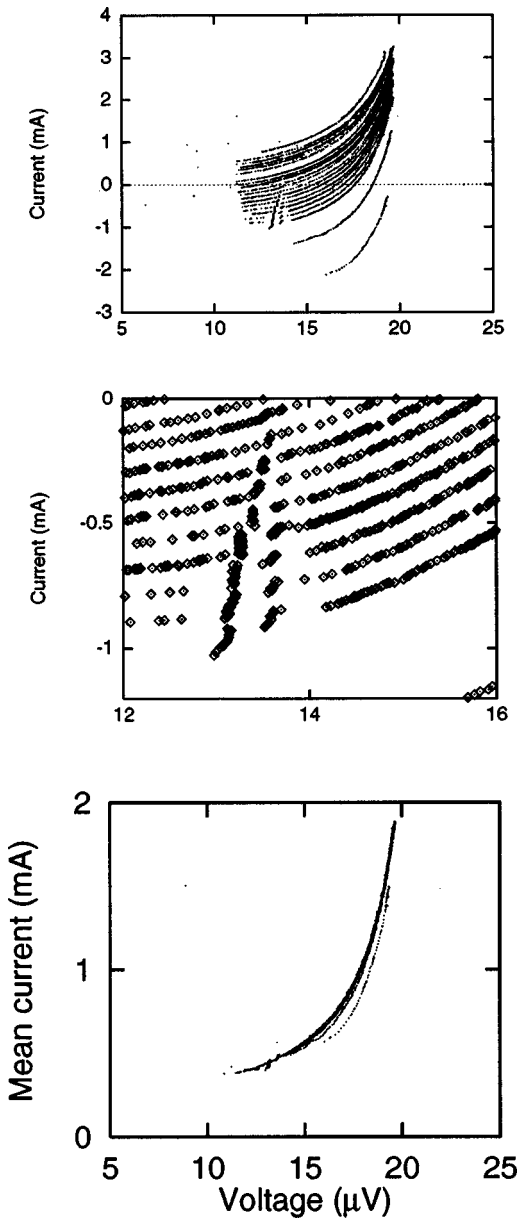

FIG. 3. Top: I-V curves of ZFS1 obtained using bias in junction A as a parameter. The current in junction A is increased from $I_A=0$ (upper curve) to $I_A=3.7$mA (lower curve). Center: Zoom of the lower branch of the step exhibiting the instability region. Bottom: All of the curves are replotted using a current axis defined by $I_s=(I_A+I_B)/2$.

investigated in the literature (see, e.g., Refs. 3–7). Here we recall some results useful to obtain information on the I-V curve of the fluxon-antifluxon state.

In normalized units and in our convention for the bias polarities, the model is

$$\varphi_{xx}-\varphi_{tt}=\sin(\varphi)+\alpha\varphi_t+\varepsilon\psi_{xx}-\gamma_A, \tag{2a}$$

$$\psi_{xx}-\psi_{tt}=\sin(\psi)+\alpha\psi_t+\varepsilon\varphi_{xx}+\gamma_B, \tag{2b}$$

$$\varphi_x(0)=\varphi_x(l)=\eta(1+\varepsilon), \tag{2c}$$

$$\psi_x(0)=\psi_x(l)=\eta(1+\varepsilon), \tag{2d}$$

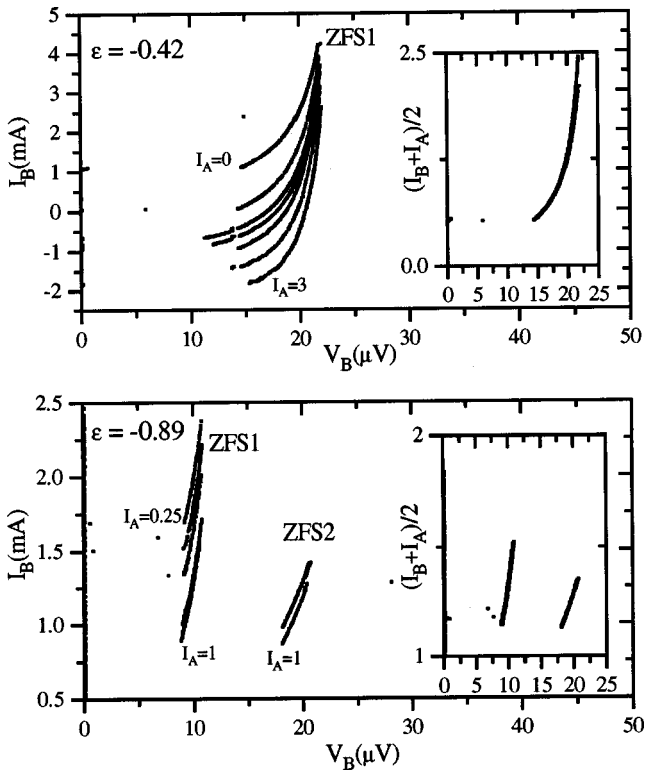

FIG. 4. Top: I-V curves of ZFS1 recorded in the stack with $\varepsilon=-0.42$ for different bias currents in junction A. The curves are replotted in the inset using the mean current axis. Bottom: Here the curves refer to the stack with $\varepsilon=-0.89$ and also ZFS2 is considered.

where $-1<\varepsilon<0$ is the magnetic coupling constant, defined as a function of the thickness d of the intermediate electrode of the stack and the thickness t of the insulating barriers by[8]

$$\varepsilon=-\frac{\lambda_L}{\sinh(d/\lambda_L)}\frac{1}{[t+\lambda_L+\lambda_L\coth(d/\lambda_L)]}.$$

The lengths in Eqs. (2) are normalized to the Josephson penetration length

$$\lambda_J=\sqrt{\frac{\hbar c^2}{8\pi e d'(1-\varepsilon^2)J_0}},$$

where $d'=t+\lambda_L+\lambda_L\coth(d/\lambda_L)$ and J_0 is the critical current density of the junctions. The time is normalized to the inverse of the plasma frequency $\omega_J=\overline{c}/\lambda_J$, where

$$\overline{c}=c\sqrt{\frac{t}{\epsilon_r d'(1-\varepsilon^2)}} \tag{3}$$

is the Swihart velocity. Again, $l=L/\lambda_J$ is the normalized length of the junctions, $\alpha=(1/R)\sqrt{\hbar/(2eCJ_0)}$ is the ohmic dissipation, and $\gamma_{A,B}=I_{A,B}/J_0LW$ are the normalized bias currents. The η term in the boundary conditions accounts for an external magnetic field H (e.g., given by a coil) applied perpendicularly to the long dimension of the stack:

$$\eta=\frac{Hc}{4\pi\lambda_J J_0(1-\varepsilon^2)}.$$

In the absence of perturbations ($\gamma_A=\gamma_B=\alpha=\eta=0$), the coupled system has the Hamiltonian (energy of the system)

$$\begin{aligned}H&=H_\varphi+H_\psi+H_I\\&=\int_{-\infty}^{\infty}\left[\frac{1}{2}\varphi_x^2+\frac{1}{2}\varphi_t^2+1-\cos\varphi\right]dx\\&\quad+\int_{-\infty}^{\infty}\left[\frac{1}{2}\psi_x^2+\frac{1}{2}\psi_t^2+1-\cos\psi\right]dx-\varepsilon\int_{-\infty}^{\infty}\varphi_x\psi_x dx,\end{aligned} \tag{4}$$

where, for the sake of simplicity, we assumed infinite length junctions. An exact solution of the unperturbed coupled system is[6]

$$\varphi=\sigma\psi=4\arctan\left\{-\exp\left[\gamma\left(\frac{u}{\sqrt{1-\sigma\varepsilon}}\right)\frac{x-ut}{\sqrt{1-\sigma\varepsilon}}\right]\right\}. \tag{5}$$

For $\sigma=1$ this solution describes a fluxon-fluxon bound state traveling with velocity u and with asymptotic velocity $u^+=\sqrt{1-\varepsilon}$, while for $\sigma=-1$ it describe a fluxon-antifluxon bound state with asymptotic velocity $u^-=\sqrt{1+\varepsilon}$. By inserting the solution in Eq. (5) into Eq. (4) we get the energy of the two bound states as

$$H_b=16\sqrt{1-\sigma\varepsilon}\,\gamma\left(\frac{u}{\sqrt{1-\sigma\varepsilon}}\right). \tag{6}$$

From Eq. (6) it is seen that the antipolar state is energetically favorable with respect to the homopolar state, but for velocities greater than about u^-. The stability of the homopolar state for the velocities between u^- and u^+ has been discussed in detail in Refs. 6 and 7 and has accounted for the existence of two characteristic velocities u^- and u^+ in the coupled system. However, probably due to the difficulty of reaching ''in flight'' the range of velocities between u^- and u^+, we did not observed this state in our stacks.

Turning to the fluxon-antifluxon state, we can obtain some information on its I-V curve using the simple energetic approach.[21] Differentiating with respect to time the energy equation (4) and by using Eqs. (2) we get

$$\begin{aligned}\frac{dH}{dt}&=\int_{-\infty}^{\infty}\gamma_A\varphi_t dx-\int_{-\infty}^{\infty}\gamma_B\psi_t dx\\&\quad-\int_{-\infty}^{\infty}\alpha\varphi_t^2 dx-\int_{-\infty}^{\infty}\alpha\psi_t^2 dx.\end{aligned} \tag{7}$$

Following the classic approach[21] we assume that the dominant perturbation is in the velocity and we assume also the existence of a stationary velocity u that makes the energy equation (6) stationary. The relevant velocity of our state is then found by inserting the fluxon-antifluxon solution in Eq. (7) with $dH/dt=0$ (power balance) to have

$$(\gamma_A+\gamma_B)\int_{-\infty}^{\infty}\varphi_t dx-2\alpha\int_{-\infty}^{\infty}\varphi_t^2 dx=0,$$

and hence

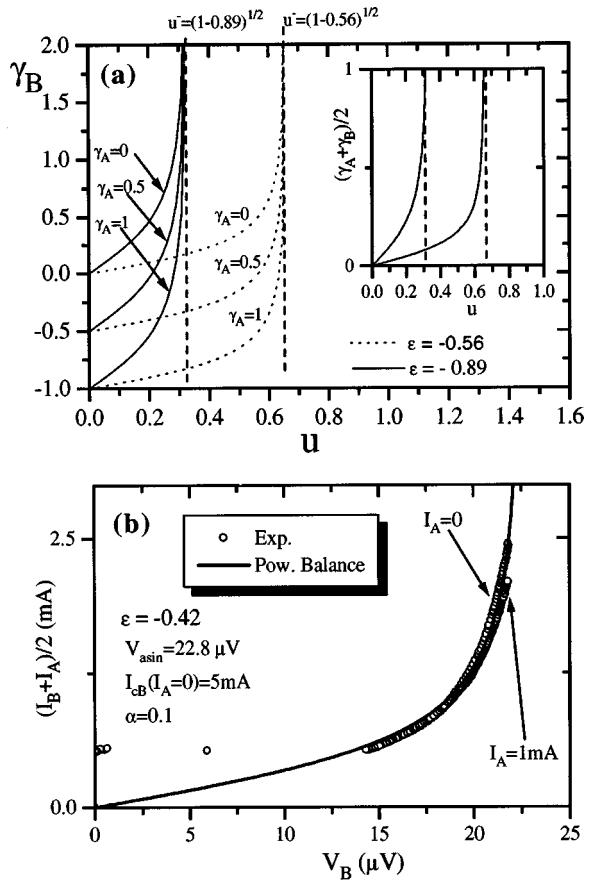

FIG. 5. Top: I-V curves of ZFS1 for two different ε as described by Eq. (8). Bottom: The experimental I-V curves of ZFS1 in the stack with $\varepsilon=-0.42$ are fitted with the power balance curve.

$$\frac{\gamma_A+\gamma_B}{2}=\frac{4\alpha}{\pi}\frac{u}{u^-}\frac{1}{\sqrt{1-(u/u^-)^2}}, \tag{8}$$

where $u^-=\sqrt{1+\varepsilon}$. By noticing that the measured voltage of ZFS1 is proportional to the stationary velocity, $V_{ZFS1}=u\Phi_0/L$, and that γ_A and γ_B are proportional to the physical bias currents, $\gamma_{A,B}=I_{A,B}/J_0LW$, Eq. (8) really describes the I-V curve of the ZFS1.

Note that Eq. (8) has been obtained assuming a perfect fluxon-antifluxon state and infinite-length junctions. Nevertheless, it describes the principal features of the experimental I-V curve. In fact, Eq. (8) predicts u^- as the asymptotic velocity of the step and the shift of the I-V curve if the bias current of one of the two junctions is used as a parameter. Moreover, from Eq. (8) it is evident that the force driving the state is the mean of the bias currents, or, in other words, that the curves must fall on top of each other if represented with the mean current axis. Global predictions of Eq. (8) are summarized in Fig. 5(a), while in Fig. 5(b) we have fitted the experimental curve with the analytical curve [Eq. (8)] obtained from the power balance.

Qualitatively, the agreement is globally satisfactory. Quantitatively, Eq. (8) does not predict a finite extension of the step, a limit originating from our assumption of infinite-length junctions in the derivation.

The experimental step at $I_A=1$mA in Fig. 5(b) seems to deviate from the analytical curve. This is because in the experimental curves we normalized both the currents to $I_{cB}(I_A=0)$, the critical current of junction B at $I_A=0$. As has been recently demonstrated,[20] the critical current of a junction depends on the current biasing the other junction in the stack. Therefore, to have better agreement we should normalize the step at $I_A=1$mA to the critical current $I_{cB}(I_A=1\text{mA})$.

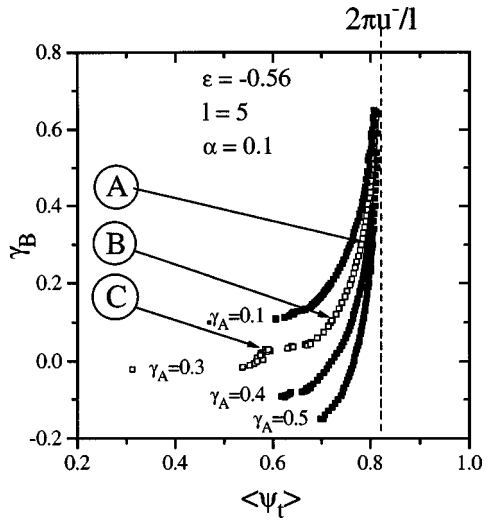

FIG. 6. ZFS1 in junction B for different currents in junction A, as obtained simulating the nonuniform model.

B. Nonuniform model

The origin of the dependence of the critical current of a junction on the current that biases the other has been accounted for by the nonuniform current distribution in the electrodes forming the double overlap stack and has been formalized in a more realistic model for the device. In our convention for the bias polarities ($\gamma_B\rightarrow-\gamma_B$), this model, that we will name the nonuniform model, is[20]

$$\varphi_{xx}-\varphi_{tt}=\sin(\varphi)+\alpha\varphi_t+\varepsilon\psi_{xx}-\eta_A(x), \tag{9a}$$

$$\psi_{xx}-\psi_{tt}=\sin(\psi)+\alpha\psi_t+\varepsilon\varphi_{xx}-\eta_B(x), \tag{9b}$$

$$\varphi_x(0)=\varphi_x(l)=\eta(1+\varepsilon), \tag{9c}$$

$$\psi_x(0)=\psi_x(l)=\eta(1+\varepsilon), \tag{9d}$$

where

$$\eta_A(x)=\frac{\gamma_A-\gamma_B}{2}+\frac{\gamma_A+\gamma_B}{2}\frac{l}{\pi\sqrt{x(l-x)}}, \tag{10a}$$

$$\eta_B(x)=\frac{\gamma_A-\gamma_B}{2}-\frac{\gamma_B+\gamma_A}{2}\frac{l}{\pi\sqrt{x(l-x)}}, \tag{10b}$$

and the other symbols have the same meaning as in the uniform current model, Eqs. (2).

In Fig. 6 is shown the ZFS1 obtained from the simulation of the nonuniform model [Eqs. (9)] with $\varepsilon=-0.56$, $\alpha=0.1$, $\eta=0$, and $l=5$. As seen in this figure, in the simula-

tions we recover also the small resonance in the lower region of the steps that appears when the bias currents are quite different.

If we depict the solitonic dynamics of the fluxon-antifluxon pair in terms of the motion of two particles in a bound state, the half sum of the bias currents gives the effective Lorentz force acting on the center of mass, while the half difference can be seen as a force opposing the internal attractive force between the antipolar solitons. If the bias currents are not so different as to break the pair, the internal motion consists of an harmonic oscillation (see, e.g., Ref. 5) around the center of mass. In the wave picture we can think of these oscillations as a perturbation to the exact solution $\varphi = -\psi$, where φ is a solitonic solution,[6,15]

$$\varphi = \phi + \delta\phi \leftarrow \text{fluxon} + \text{perturbation},$$

$$\psi = -\phi + \delta\phi \leftarrow \text{antifluxon} + \text{perturbation}. \tag{11}$$

This ansatz reduces the model, Eqs. (9), to

$$(1+\varepsilon)\,\phi_{xx} - \phi_{tt} - \sin\phi\cos\delta\phi = \alpha\phi_t - \frac{\gamma_A+\gamma_B}{2} - \frac{l}{\pi\sqrt{x(l-x)}}, \tag{12a}$$

$$(1-\varepsilon)\,\delta\phi_{xx} - \delta\phi_{tt} - \sin\delta\phi\cos\phi = \alpha\delta\phi_t - \frac{\gamma_A-\gamma_B}{2}. \tag{12b}$$

From Eqs. (12) it is clearly seen that the solitonic component of the solution, moving with asymptotic velocity u^-, is driven by the half sum of the bias while the perturbation, moving with asymptotic velocity u^+, is driven by the half difference of the bias currents. In the nonuniform model the driving force of the solitonic component is also spatially modulated, inducing possible resonances.

Due to the form of the ansatz, the perturbations are in phase in the two junctions. In Fig. 7 we show the dynamics in the three points of ZFS1 at $\gamma_A = 0.3$ marked in Fig. 6. In the figure we report the instantaneous voltage profiles (φ_t and ψ_t), and their half sum and half difference, that, from Eqs. (11), describe the perturbation and the solitonic component, respectively. In the *A* state the bias currents are identical, and, consistently, there is no perturbation. The perturbations are small, and approximatively in phase, in the *B* state, where bias currents are only slightly different. In the *C* state the bias currents are quite different: the perturbations are large and overcome the solitonic component.

IV. STABILITY RANGE

As implicitly asserted in the last section, ZFS1 recorded in a junction exists for many values of the fixed bias current in the other junction, i.e., the fluxon-antifluxon state does not require necessarily equal bias currents to exist. We characterized[15,17] this feature by measuring the current ranges for which the two junctions persist in the voltage range associated to ZFS1. The experimental procedure is the following: once the paired state has been established, the bias current in one junction is kept constant, while the other is varied until the junctions switch to the zero-voltage state or to the McCumber curve; hence, the currents of the switching point are recorded. We emphasize that the procedure identifies reliably the stability range of the fluxon-antifluxon pair. In fact, we never found that the junctions could be biased each on its own ZFS1 without being, at same time, voltage locked; in other words, both the binding and the breaking of the pair occur apparently as fast transitions, not as the smooth evolution of two independent solitonic states. With reference to Fig. 8(a), the fluxon-antifluxon state exists in the interior of the closed curve in the I_A-I_B plane. The driving role played by the half sum and the destructive role played by half difference of the bias current is clarified by the representation of the same data in the inset of Fig. 8(a): the stability of the state (extension of the step) decreases as the half difference of bias currents increases. In both representations, we can note experimental points in the interior of the stability range. They are due to the small resonance in the lower branch of the ZFS1 previously discussed.

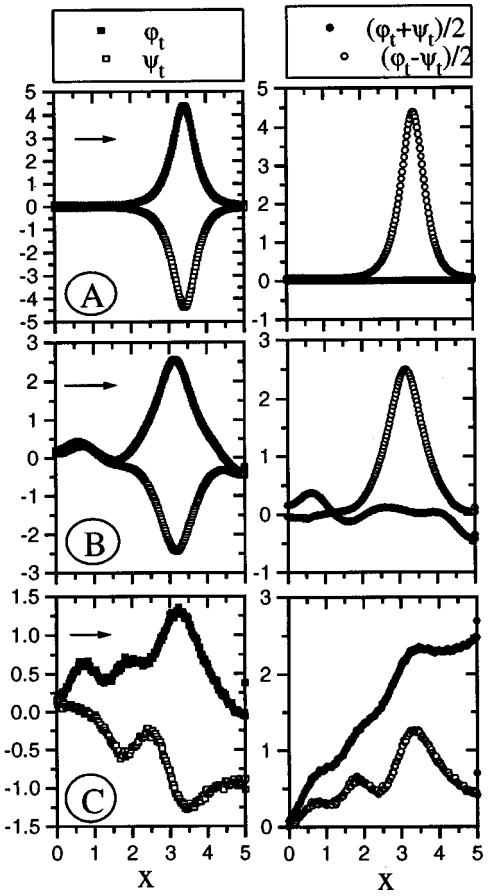

FIG. 7. Dynamics in the points of ZFS1 marked in Fig. 6. Note that in this plot the voltage of junction *B* is not referred to the intermediate electrode.

In Fig. 8(b) are shown the stability ranges of ZFS1 (Ref. 17) and of the ZFS2 as a function of an applied magnetic field. The behavior is similar to the behavior observed in the single junctions: the maximum step extension is obtained always at zero magnetic field.

For a quantitative comparison with the theory we simulated the nonuniform model, Eqs. (9), where we recall that η is proportional to the applied magnetic field.

To obtain the stability range at zero field we integrated the model, Eqs. (9), with $\eta = 0$ starting with an initial condition of a fluxon in a junction and an antifluxon in the other. When

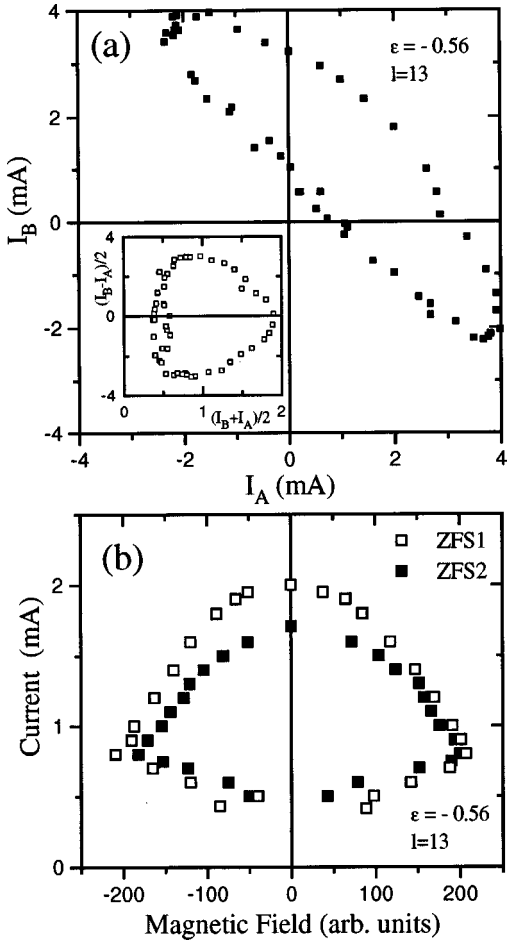

FIG. 8. (a) Stability range of ZFS1 in the plane of the bias currents. In the inset the same data are replotted in the plane of the half difference and the half sum of the bias currents. (b) Magnetic-field patterns of ZFS1 and ZFS2 biased with equal currents.

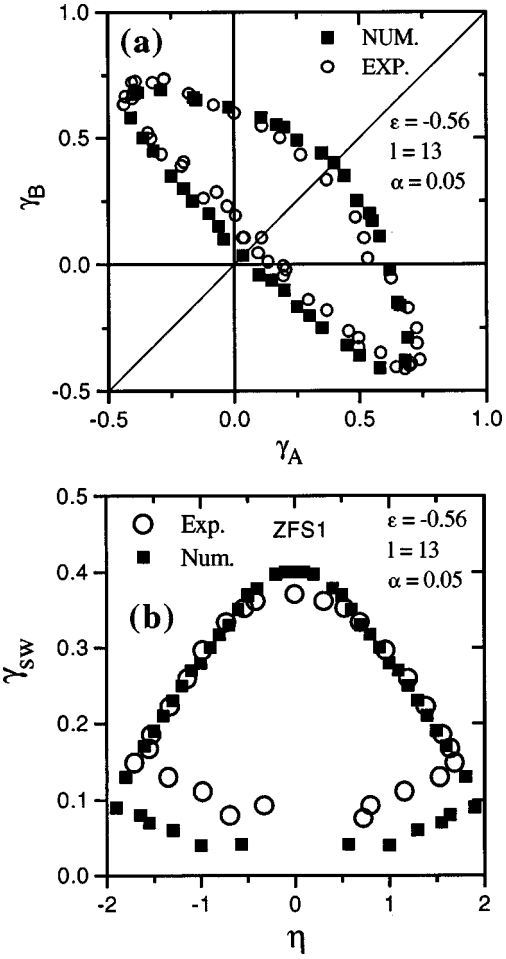

FIG. 9. (a) Comparison between the experimental and numerical stability range of ZFS1. (b) Numerical and experimental magnetic-field pattern of ZFS1.

a stationary oscillatory motion of the pair was reached with a certain configuration of the bias, the bias currents were varied following some path in the γ_A-γ_B plane until the bound state was lost. The point in the γ_A-γ_B plane corresponding to the last event was obviously a point of the stability boundary of ZFS1. In Fig. 9(a) the numerical stability range is compared with the experimental one for the stack with $\varepsilon=-0.56$. To allow a direct comparison, the parameters in the simulations were taken from the experimental data. To simulate the behavior of ZFS1 as a function of the magnetic field, we fix $\eta\neq 0$ in Eqs. (9), we start with a fluxon-antifluxon pair, and we vary the common value of bias currents ($\gamma_A=\gamma_B=\gamma$) until the bound state is lost at some critical current value γ_{sw}. As an alternative procedure, practically necessary to obtain the lower region of the stability range (mimicking the one used in the experiments), we fix some value of γ for which the ZFS1 exists at $\eta=0$, and then we increase the magnitude of η until the bound state is lost. Numerical and experimental stability ranges in magnetic field are compared in Fig. 9(b). For a similar comparison in the framework of the uniform model, Eqs. (2), see Fig. 6 in Ref. 17. The slightly reduced experimental range with respect to the numerical one evident in Fig. 9 is essentially due to the absence of the β parameter in the model, Eqs. (9). In fact, this term, that accounts for the surface impedance of the superconducting electrodes, is known to play a meaningful role in the extension of the ZFS's of the single junctions and also for the ZFS's in the stacks. However, results in Fig. 9 suggest that the model, Eqs. (9), describes the experimental behavior quite well also in this less refined version.

An approximate stability range in zero magnetic field has been analytically derived in Ref. 5. For the fluxon-antifluxon pair, and with our convention for the bias polarities, the stability range is defined by the two limit curves in the plane of half sum and half difference of the bias currents (see Fig. 10):

$$\left|\frac{\gamma_A-\gamma_B}{2}\right|<1-\frac{\gamma_A+\gamma_B}{2}, \tag{13}$$

$$\left|\frac{\gamma_A-\gamma_B}{2}\right|<\frac{4}{3\pi}|\varepsilon|\left[1+\left(\frac{\pi}{4\alpha}\frac{\gamma_A+\gamma_B}{2}\right)^2\right]. \tag{14}$$

Notice that relation (13) follows from trivial conditions that the ZFS1 cannot be higher than the Josephson critical current $I_0=J_0LW$, i.e., from definition of $\gamma_{A,B}$, $|\gamma_A|<1$ and $|\gamma_B|<1$.

These limit curves were obtained for infinite length junctions using the uniform model, Eqs. (2). Obviously, due to the deviation of the experimental device from the ideal uni-

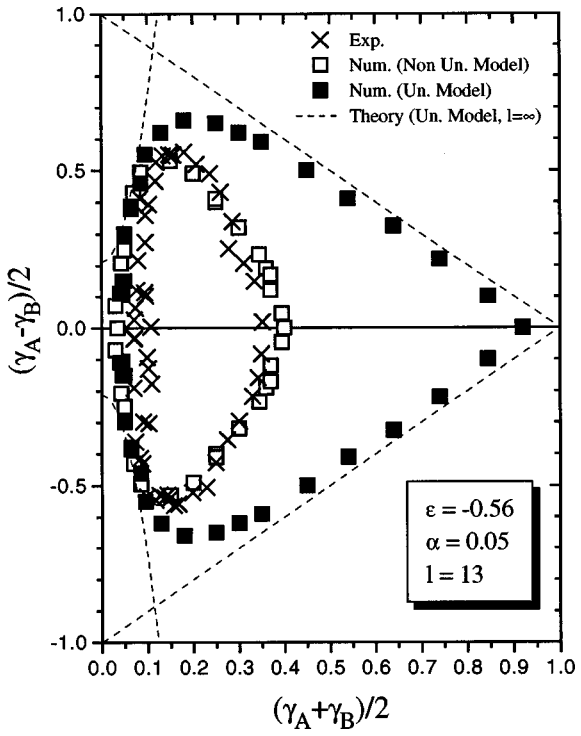

FIG. 10. Comparison of the experimental stability range with the analytical curves, Eq. (13) and Eq. (14), and with the numerical results of the uniform as well as the nonuniform model for finite-length junctions.

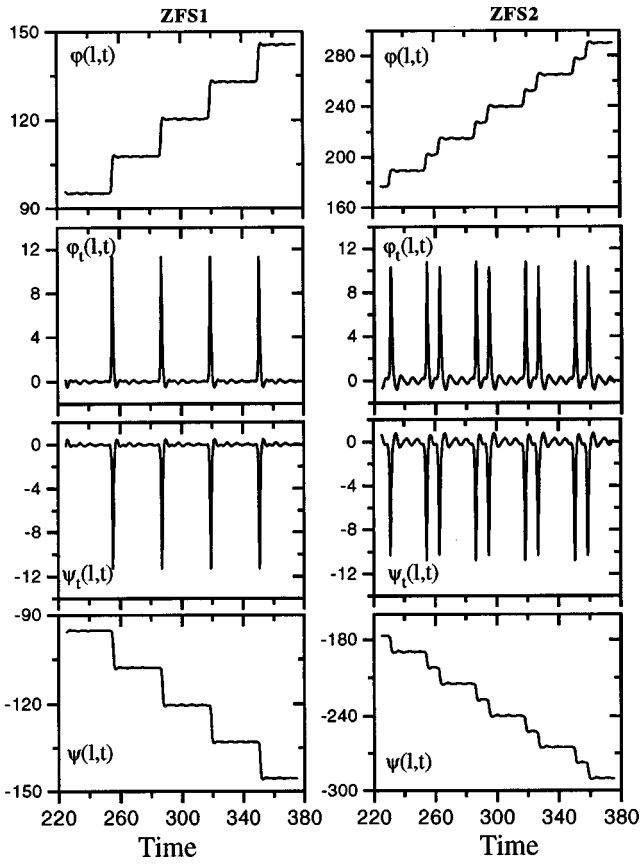

FIG. 11. Instantaneous phases and voltages at one edge of the stack while the junctions are on ZFS1 (to the left) or on ZFS2 (to the right). In the simulations are $\varepsilon=-0.56$, $l=10$, $\alpha=0.1$, $\gamma_B=\gamma_A=0.37$.

form model, we can expect only qualitative information from curves (13) and (14), e.g., the form of the stability range and its dependence on relevant physical parameters. For a self-explicative comparison, the analytical stability range, the numerical results of the uniform model and of the nonuniform model for finite-length junctions, and the experimental results are all compared in Fig. 10.

V. MICROWAVE RADIATION FROM THE ZFS'S

When we bias the stack on the ZFS's at the edge of a junction of the stack a periodic voltage signal is established, as seen in the numerical results shown in Fig. 11. The fundamental frequency of the voltage signal is $f_0=u/2L$, related to the dc component by the well-known relation

$$f_0=\frac{1}{2}483.6\frac{MHz}{\mu V}\frac{V_{ZFSN}}{N}, \tag{15}$$

where N is the order of the ZFS.

We performed measurements to detect radiation from the ZFS's of our stacks. The results for the stack with $\varepsilon=-0.56$ are summarized in Fig. 12, where the power spectra of the radiation received from ZFS1, ZFS2, ZFS4, ZFS5, ZFS6 are shown. Apart from the spurious spectral components (due to an instrumental effect), the fundamental frequency of the emitted signal is found to satisfy very well relation (15). In Fig. 12 we also reported a *current-frequency* curve of the upper branch of the ZFS1. From relation (15) this curve corresponds to a *current-voltage* curve recorded with an accuracy in the voltage good enough to evidentiate possible fine structures in the I-V curve that, as seen in the figure, are not exhibited by our ZFS1.

The calculated wave forms of the signals (see Fig. 11) have a wide Fourier spectrum, with the amplitude of the higher-order harmonics almost comparable to the amplitude of the first (fundamental) harmonic. Due to the limitation of our experimental setup, we could detect up to the second harmonic of the signals. In Fig. 13 there are reported the power spectra of the fundamental and the second harmonic of the signals detected from ZFS1 and ZFS2 of the stack with $\varepsilon=-0.56$. Note that the spectra in Figs. 12 and 13 were obtained biasing the junctions with different currents. However, similar results were obtained biasing the junctions with the same currents.

Looking at the waveforms in the Fig. 11 we conclude that the net signal generated at the edge of the stack should be the sum of nearly opposite signals and consequently too small to be detected. Nevertheless, we received appreciable radiation from the ZFS's. Why? Possibly, the explanation could be looked for in the impulsive nature of the signals. In fact, a suitable time delay τ between the signals would generate an appreciable net signal. In particular, a time delay τ of the order of the impulse width Δt would generate a net signal with the same frequency and with doubled amplitude with respect to the component signals, as shown in Fig. 14. As seen in the Fig. 11, the width Δt of the impulse is estimated to be about some percent of the signal period T. Due to the

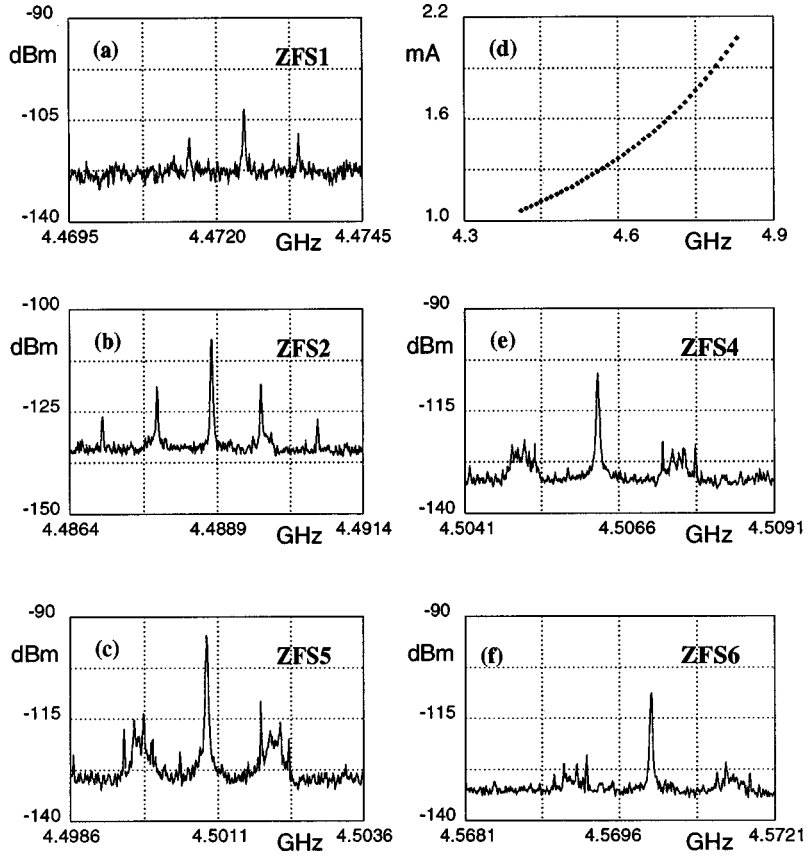

FIG. 12. Power spectra of the radiation received from ZFS's. The radiation is recorded at voltages (a) 18.5 μV, (b) 37.1 μV, (c) 92.2 μV, (e) 72.0 μV, (f) 112.0 μV. In (d) is shown the *current-frequency* curve of the upper branch of ZFS1.

Lorentz contraction, this width can be reduced to 0.1% T when we approach the asymptotic voltage of the steps. To quantify, if $\tau \sim \Delta t \approx 10^{-3} \times T - 10^{-2} \times T$ we could expect a net signal significantly other than zero. For a fundamental frequency $f_0 = 4.5$GHz, as it is in our case, according to the experimental data, the delay should be

$$2 \times 10^{-13} \text{ s} < \tau < 2 \times 10^{-12} \text{ s}. \tag{16}$$

At a first glance, such a time delay could be guessed to originate from the internal motion of the pair enhanced by nonidentical parameters of the junctions in the stack. In fact, in Fig. 11 the numerical signals were obtained assuming

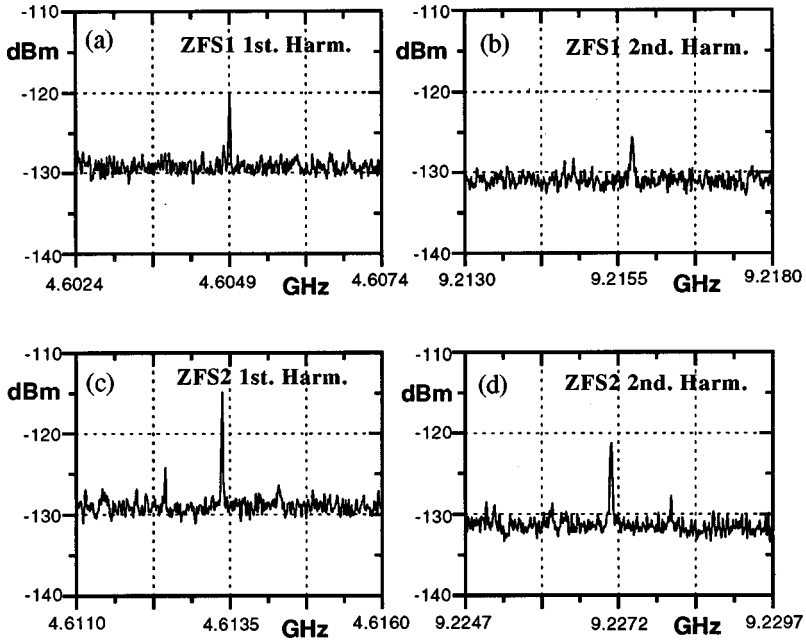

FIG. 13. First and second harmonic power spectra of the radiation received from ZFS1 and ZFS2.

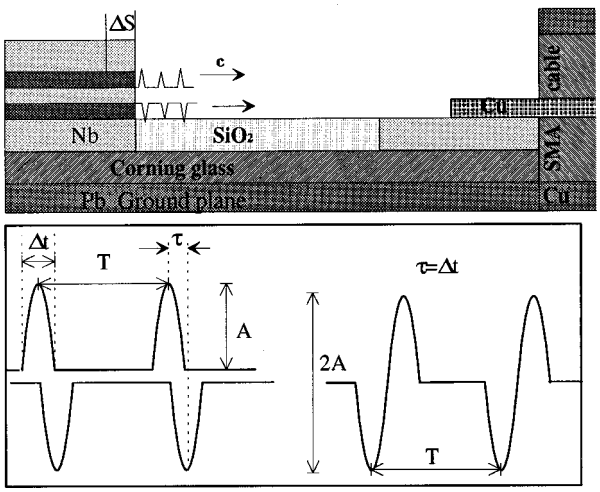

FIG. 14. Top: Sketch of the receiving circuitry. Bottom: Possible construction of an appreciable net signal by means of a suitable time delay.

identical junctions and equal bias currents, so that the internal motion was minimized. Nevertheless, also simulating the more realistic case of slightly different junctions biased with different current, we always found that the net signal generated by the fluxon-antifluxon pair was vanishingly small. A time delay of the right order of magnitude could be originated, instead, if the junctions had different physical lengths. This is very likely to happen, because the photolithographic process defining the junctions has the resolution of a few micrometers. Supposing that one of the electrodes has a length $L' = L - \Delta S$, one junction of the stack will have the same length and the other will be longer. Just after the emission, the signal of the shorter junction will propagate in the air at velocity c, while the other will propagate for a distance ΔS at velocity $\bar{c} = kc \approx 0.01c$ in the longer junction (see Fig. 14). Assuming a realistic $\Delta S \approx 3\mu$m, the produced time delay between the signal would be

$$\tau = \frac{\Delta S}{c}\left(\frac{1}{k} - 1\right) \approx 10^{-12} \text{ s},$$

that is, of the right order to generate an appreciable net signal. We note that, on the basis of this interpretation, we expect to observe radiation principally in the higher branch of the steps, where Lorentz contraction makes possible the construction of a net signal also for small time delays. This is really observed in the experiments.

We conclude noticing that, if this explanation based on a fortuitous time delay is correct, we have luckily found a way to convert the opposite signals generated by the fluxon-antifluxon state into a net signal with approximately doubled amplitude, i.e., a design criterion to generate radiation of appreciable power from the fluxon-antifluxon state.

ACKNOWLEDGMENTS

I am greatly indebted to Professor G. Costabile for his help in this research and for his assistance during the preparation of this paper. The experimental setup and the stimulating assistance and discussions with Professor J. Mygind are gratefully acknowledged as well as the fruitful scientific collaboration with Professor N. F. Pedersen. Useful discussions with Professor M. R. Samuelsen and collaborations with Dr. A. Petraglia, Dr. G. Filatrella, M. Manscher, and M. Nordhan are also acknowledged. Finally, I thank the Department of Physics of the Technical University of Denmark for the warm hospitality.

[1] M. B. Mineev, G. S. Mkrtchjan, and V. V. Schmidt, J. Low Temp. Phys. **45**, 497 (1981).
[2] A. F. Volkovra, Pis'ma Zh. Eksp. Teor. Fiz. **45**, 299 (1987) [JETP Lett. **45**, 376 (1987)].
[3] Y. Kivshar and B. Malomed, Phys. Rev. B **37**, 9325 (1988).
[4] Y. Kivshar and B. Malomed, Rev. Mod. Phys. **61**, 763 (1989).
[5] N. Grønbech-Jensen, M. R. Samuelsen, P. S. Lomdahl, and J. A. Balckburn, Phys. Rev. B **42**, 3976 (1990).
[6] N. Grønbech-Jensen, D. Cai, and M. R. Samuelsen, Phys. Rev. B **48**, 16 160 (1993).
[7] N. Grønbech-Jensen, D. Cai, A. R. Bishop, A. W. C. Lau, and P. S. Lomdahl, Phys. Rev. B **50**, 6352 (1994).
[8] S. Sakai, P. Bodin, and N. F. Pedersen, J. Appl. Phys. **73**, 2411 (1993).
[9] N. Grønbech-Jensen, J. A. Blackburn, and M. R. Samuelsen, Phys. Rev. B **53**, 12 364 (1996).
[10] R. D. Parmentier, P. Barbara, G. Costabile, A. D'Anna, B. A. Malomed, and C. Soriano, Phys. Rev. B **55**, 15 165 (1997).
[11] A. V. Ustinov, H. Kohlsted, M. Cirillo, N. F. Pedersen, G. Hallmanns, and C. Heiden, Phys. Rev. B **48**, 10 614 (1993).
[12] A. V. Ustinov, H. Kohlstedt, and C. Heiden, Appl. Phys. Lett. **65**, 1457 (1994).
[13] P. Barbara, A. Ustinov, and G. Costabile, Phys. Lett. A **191**, 443 (1994).
[14] S. Sakai, A. V. Ustinov, H. Kohstedt, A. Petraglia, and N. F. Pedersen, Phys. Rev. B **50**, 12 905 (1994).
[15] G. Carapella, G. Costabile, A. Petraglia, N. F. Pedersen, and J. Mygind, Appl. Phys. Lett. **69**, 1300 (1996).
[16] G. Carapella, G. Costabile, M. Manscher, and M. Nordham, J. Low Temp. Phys. **106**, 345 (1997).
[17] G. Carapella, G. Costabile, G. Filatrella, M. Manscher, J. Mygind, M. Nordhan, N. F. Pedersen, and A. Petraglia, IEEE Trans. Appl. Supercond. **7**, 2411 (1997).
[18] G. Carapella and G. Costabile, Appl. Phys. Lett. **71**, 3409 (1997).
[19] G. Carapella and G. Costabile, Appl. Phys. Lett. **72**, 377 (1998).
[20] G. Carapella, G. Costabile, S. Sakai, and N. F. Pedersen, Phys. Rev. B **58**, 6497 (1998).
[21] D. W. McLaughlin and A. C. Scott, Phys. Rev. A **18**, 1652 (1978).